SLAC-PUB-2894
March 1982
(E/I)

THE MAC CALORIMETERS AND APPLICATIONS*

MAC Collaboration:
Colorado-Frascati-Northeastern-SLAC-Utah-Wisconsin†
Presented by W. T. Ford, Colorado

Summary

The MAC detector at PEP features a large solid-angle electromagnetic/hadronic calorimeter system, augmented by magnetic charged-particle tracking, muon analysis and scintillator triggering. Its implementation in the context of electron-positron annihilation physics is described, with emphasis on the utilization of calorimetry.

Detector Description

The MAC detector is shown in Fig. 1. Charged particles produced with polar angles between 17° and 163° are analyzed in the central tracking chamber, which comprises 833 drift cells arranged as 10 layers in a common gas volume. Each cell contains a double sense-wire pair connected to differential electronics so that drift distance is determined without right-left ambiguity. The wires in four of the layers are axial; these are interspersed with six stereo layers at plus and minus three degrees to determine axial positions. The setting accuracy is 200 μm; with the solenoidal magnetic field of 5.7 kG, the momentum resolution is $\Delta p/p \simeq .065\ p \sin\theta$.

Surrounding the solenoid coil is the central shower chamber (referred to below as SC), a calorimeter optimized for electromagnetic shower analysis and composed of 32 lead plates interspersed with proportional wire chambers for a total thickness of 16 radiation lengths. Each anode wire is suspended parallel to the beam at the center of a rectangular aluminum cathode about 1 cm thick × 2 cm wide. Groups of wires are combined for readout as 192 azimuthal sectors in each of three layers. Axial position is determined by current division, i.e., the ratio of pulse heights measured at both ends of the wire group through low input-impedance preamplifiers.

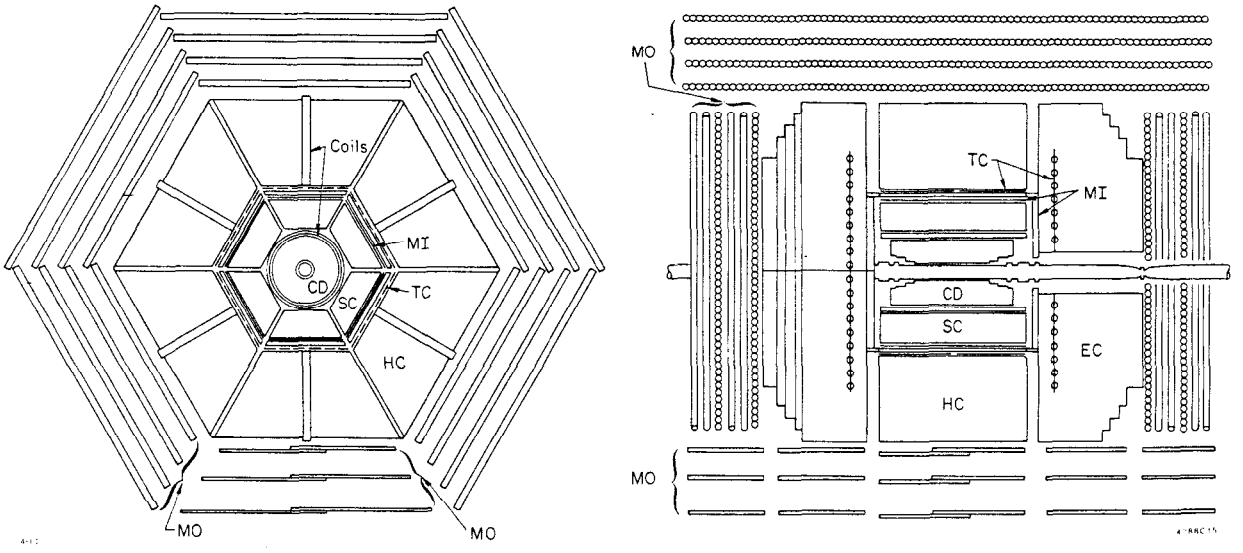

Fig. 1. MAC detector layout. The components labelled in the figure are: central drift chamber (CD), shower chamber (SC), trigger/timing scintillators (TC), central and endcap hadron calorimeters (HC, EC), and the inner and outer muon drift chambers (MI, MO). Also indicated are the solenoid and toroid coils.

*Work supported in part by the U. S. Department of Energy, under contract numbers DE-AC02-76ER02114, DE-AC03-76SF00515, and DE-AC02-76ER00881, by the National Science Foundation under contract numbers NSF-PHY77-21210, NSF-PHY77-21297, and NSF-PHY5-39485, and by I. N. F. N.

†MAC Collaborators are: W. T. Ford, J. S. Marsh, A. L. Read, J. G. Smith, Department of Physics, University of Colorado, Boulder, CO 80309; A. Marini, I. Peruzzi, M. Piccolo, F. Ronga, Laboratori Nazionali Frascati dell' I.N.F.N. (Italy); K. Appert, L. Baksay, H. R. Band, W. L. Faissler, M. W. Gettner, G. P. Goderre, B. Gottschalk, R. B. Hurst, O. A. Meyer, J. H. Moromasato, W. D. Shambroom, E. von Goeler, Roy Weinstein, Department of Physics, Northeastern University, Boston, MA 02115; J. V. Allaby, W. W. Ash, G. B. Chadwick, S. H. Clearwater, R. W. Coombes, Y. Goldschmidt-Clermont, H. S. Kaye, K. H. Lau, R. E. Leedy, S. P. Leung, R. L. Messner, S. J. Michalowski, K. Rich, D. M. Ritson, D. E. Wiser, R. W. Zdarko, Stanford Linear Accelerator Center, Stanford University, Stanford, CA 94305; D. E. Groom, Hoyun Lee, E. C. Loh, Department of Physics, University of Utah, Salt Lake City, UT 84112; M. C. Delfino, M. Frankowski, B. K. Heltsley, J. R. Johnson, T. Maruyama, R. M. Morse, R. Prepost, Department of Physics, University of Wisconsin, Madison, WI 53706.

(Presented at the SLAC International Conference on Instrumentation for Colliding Beams, Stanford, California, February 17-23, 1982.)

The central hadron calorimeter (HC) which surrounds the shower chamber has a very similar structure except the absorbers are 24 1-inch-thick steel plates, followed by three 4-inch-thick plates. The three thick plates and their associated proportional chambers are for muon tagging.

The steel plate calorimeter is extended to small polar angles by the two endcap sections (EC), whose absorber plates stand perpendicular to the beam. Each endcap has 28 1-inch-thick calorimeter plates followed by 2 4-inch-thick muon tagging layers. The endcap sampling detectors are planar proportional chambers, each covering a 30-degree azimuthal sector. The anode wires run parallel to the edges of the hexagonal endcaps and are grouped, for readout, into four radial panels. Each cathode is divided into three 10-degree azimuthal wedges which are read out as well. The chambers occupying the first 9 gaps (16 radiation lengths) have finer segmentation to match them to the electromagnetic showers which are outside the acceptance of the central shower chamber. In these chambers each segment measures about 5° in azimuth by 5° in zenith. The endcap signals are grouped into four layers in depth.

One layer of scintillation counters for triggering and time-of-flight are inserted into one gap near the entrance face of the hadron calorimeter, in the central and both endcap regions. There are 144 separate scintillators.

The muon tracking system consists of one central and three endcap planes of drift chambers located before the entance faces of the hadron calorimeter, four layers of drift chambers surrounding the calorimeter, and six layers covering the end faces. For momentum analysis the calorimeter/absorber steel is magnetized by toroid coils, one at the center of each sextant. The entrance chambers, and those underneath the calorimeter, are planer; the remaining exit planes are assembled from 10-cm-diameter tubes each containing a single wire. The wires are all oriented to determine axial position, since the toroidal field causes a change in the tracks' polar angle, except for the endcap planes of which two layers have horizontal wires, and two each have wires at 60° and 120° respectively.

Triggers for the experiment may be summarized, with some simplification, as the logical OR of: (1) scintillator opposite sextants or end quadrants; (2) scintillator hits on any 3 or more of the 8 faces of the hexagonal prism with ends; (3) showers of at least 2 GeV in any 2 of: 6 SC sextants, 2 endcaps, or any part of the HC; (4) one or more penetrating tracks, defined by a string of central drift hits within a 20° sector and the corresponding scintillator and central hadron calorimeter sextant registering at least 400 MeV.

Calibration and Resolutions

The electromagnetic calorimeters have been calibrated with electrons from Bhabha scattering. The energy response for the central shower counter is shown in Fig. 2. The observed width of 8% (standard deviation) is greater than the 5% we would expect on the basis of earlier tests with one of the sextants in an electron beam. Those tests gave $\Delta E/E \simeq .20/\sqrt{E}$ from .5 to 16 GeV. The difference is largely attributable to scattered non-functioning channels which number about 3-7% of the total. (The curve accompanying the data of Fig. 2 includes the effect of 5% randomly-distributed non-responding channels.) Presumably the importance of this effect is smaller at lower energies relative to inherent ionization fluctuations. In any case, the resolution of this device is not the limiting one for hadron calorimetry. The directional resolution, measured by comparing the shower centroid with the extrapolated central drift chamber track, is 0.8° in ϕ × 1.3° in θ. The ϕ error corresponds to about 0.4 times the wire group segmentation. The θ error corresponds to about 1% of the wire length from current division.

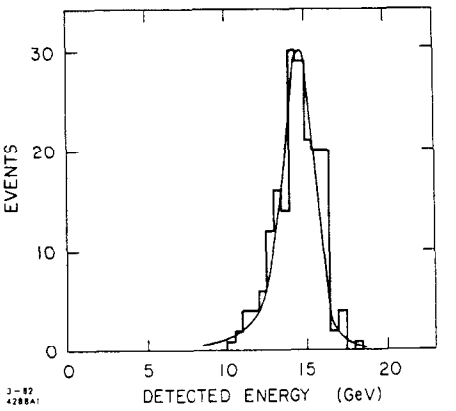

Fig. 2. Energy response of the central shower chamber to 14.5-GeV electrons. The curve is the predicted resolution function.

The corresponding information for the endcap shower chamber is presented in Fig. 3. The low-energy tail in Fig. 3a is caused by the insensitive regions occupied by the frames of the proportional chambers. These regions occur every 30 degrees and are about 10 cm wide, independent of radius, and hence have maximum impact near the poles which are preferentially illuminated by the Bhabha electrons. The directional resolution is 2° in ϕ (cathode strips) × 1.5° in θ (anode wire groups).

The shower detectors alone accomplish both triggering and analysis of $\gamma\gamma$ events, for which we show, in Fig. 4, the noncollinearity angle distribution compared with the QED calculation.

For calibration of the response of the calorimeter system to hadrons, we have only the total energy of multihadron events as a known reference point. To produce the corresponding measured total pulse height, we

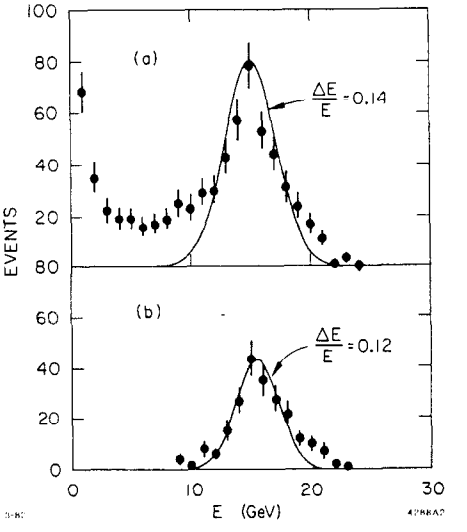

Fig. 3. Energy response of the endcap calorimeter to 14.5-GeV electrons for (a) all azimuthal angles, and (b) events within fiducial area.

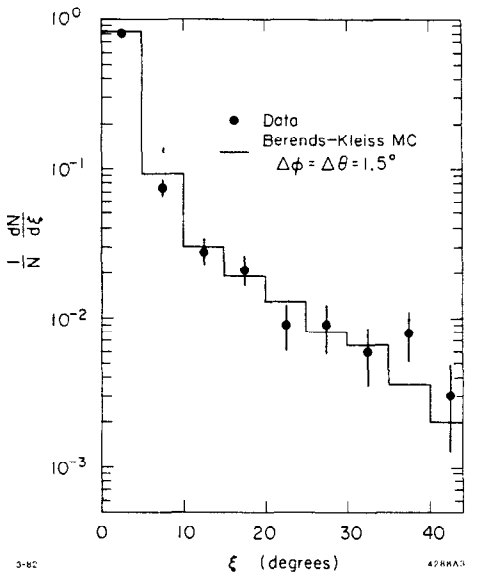

Fig. 4. Noncollinearity angle distribution for $ee \to \gamma\gamma$.

must bring into register the three separate calorimeters (SC, HC and EC), for samples containing a fluctuating mixture of hadrons and gammas from neutral pion decay incident over a wide range of entrance angles. The response to gammas per GeV will presumably be the same as that measured for electrons; for incident hadrons we expect an average of about 30-40% of the energy is lost to nuclear binding and heavily ionizing fragments. With these expectations in mind, we may write

$$a\ P(SC)_i + b\ P(HC)_i + c\ P(EC)_i = E_{cm},$$

where a, b, and c are the factors for converting each calorimeter's pulse height, P, into energy units, and i is the event index. (In general one may treat separately the several layers within SC, etc., as well.) The coefficients are determined by a fit to all the events in the multihadron sample.

The measured response to multihadron events with narrow jet structure and thrust axis pointed toward the central calorimeter is given in Fig. 5a. For comparison, Fig. 5b shows results of a calculation using the Monte Carlo programs EGS[1] and HETC[2] with our geometry. Both curves give $\Delta E/E \simeq .16$. We may compare this with our earlier beam tests of a model of the HC alone with pions of several energies at normal incidence. These can be summarized as $\Delta E/E = .75/\sqrt{E}$, which gives .14 at 29 GeV. The corresponding results for $37° \leq \theta_{thrust} \leq 143°$ which covers all three calorimeters but avoids losses near the poles, are shown in Fig. 6. In this case, we get $\Delta E/E \simeq .18$, and again our results agree quite well with the calculation.

The directional resolution for hadrons is set by the spread of the hadronic cascade in the calorimeters. One measure of this is the mass of a hadron jet. The hadronic decays of tau leptons provide a sample of known, limited mass: $m_\pi \leq m_{jet} \leq m_{tau} = 1.8$ GeV. The mass determined for such events by calorimetry is shown in the distribution of Fig. 7a. This resolution function is narrow compared with the distribution for multihadron events seen in Fig. 7b.

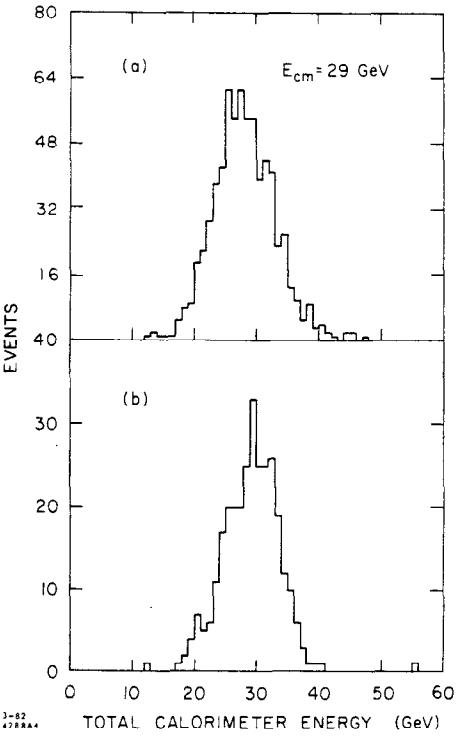

Fig. 5. Total energy of multihadron events, central region: (a) data; (b) Monte Carlo calculation.

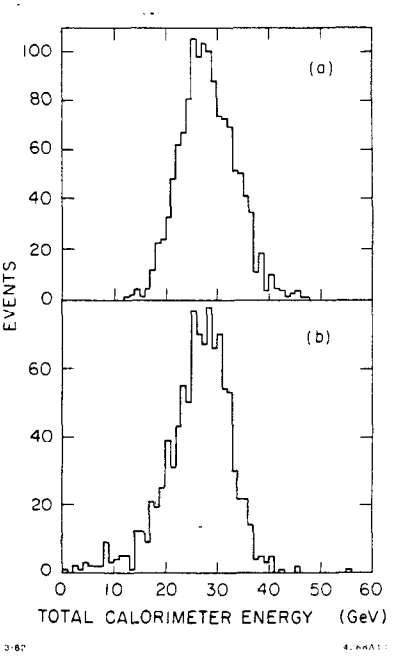

Fig. 6. Same as Fig. 5 for all non-polar events.

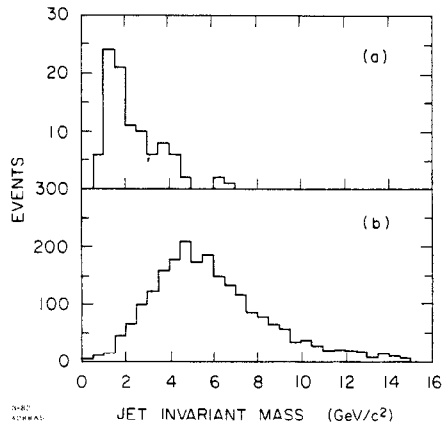

Fig. 7. Invariant mass of one jet for (a) hadronic τ decays, and (b) multihadron events.

Multihadron Event Section

The large acceptance calorimeter system is well suited to the efficient extraction of multihadron events from single photon annihilation of electrons and positrons, even in the presence of copious multihadron production by two-photon annihilation. The solid histogram of Fig. 8 shows the raw distribution in total visible energy of all events triggering the experiment and having at least five charged prongs forming a vertex within the interaction volume of the colliding beams. For one-photon events the total visible energy 4-vector is, except for measurement error, very nearly that of the initial state, i.e., energy = 2 E_{beam}, and net momentum = 0. The two-photon events have two final-state electrons carrying a substantial fraction of energy generally outside the acceptance of the detector (typically inside the vacuum pipe). The visible 4-vector therefore has energy less than 2 E_{beam} net momentum along the beam direction, and limited momentum perpendicular to the beam. We measure the net motion of the visible energy by the imbalance vector,

$$\vec{\beta} = \sum E_i \hat{n}_i / \sum E_i,$$

and the perpendicular energy by

$$E_\perp = \sum E_i \sin\theta_i,$$

where E_i is the energy, θ_i the polar angle, and $\hat{n}_i$ the unit direction vector for energy parcel i. Fig. 9a and b show the distributions in $\beta = |\vec{\beta}|$ and $E_\perp$, respectively, for the event sample plotted in Fig. 8. The indicated cut in β (Fig. 9a) is chosen to remove a substantial fraction of background without reducing the signal significantly. The cut in $E_\perp$ (Fig. 9b) does take out that fraction of the signal which is essentially indistinguishable from background; it amounts to an acceptance loss, estimated to be about 5% of all one-photon events. After application of several selection criteria of which the foregoing are the most important, the distribution in total visible energy is decomposed into the signal and background parts indicated by the dashed and dotted histograms in Fig. 8.

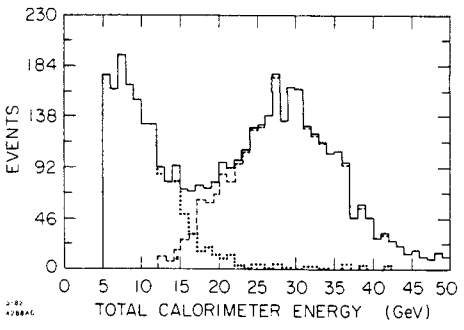

Fig. 8. Total evergy for all ≥5-prong events. The dashed histogram represents events passing the selection criteria for multihadron events; events in the dotted histogram are the remainder.

An alternative analysis (method 2) has been performed which accomplishes this decomposition of the multihadron sample by fitting signal and background shapes to the total distribution with adjustable scale factors. The parent shapes were extracted by requiring more than 8 prongs and small β_z to get the signal function and by taking events with large β_z to model the background (see Fig. 10). The full distribution was cut near the minimum between the two peaks and the fitted components used to estimate the loss of signal and the residual background.

The event yields which result from these analyses for a particular data collection period (representing a subset of the data of Fig. 8) are:

$$N = 1839 \pm 45 \text{ (Method 1)}$$

$$N = 1801 \pm 49 \text{ (Method 2)}.$$

We expect that with improved statistical precision, yield measurements accurate within 2-3 percent should be possible. The model-dependent acceptance correction is very small; a precise measurement of $R = \sigma_{hadron}/\sigma_{\mu\mu}$ should be possible, assuming such factors as the luminosity, radiative corrections, etc. are also well understood.

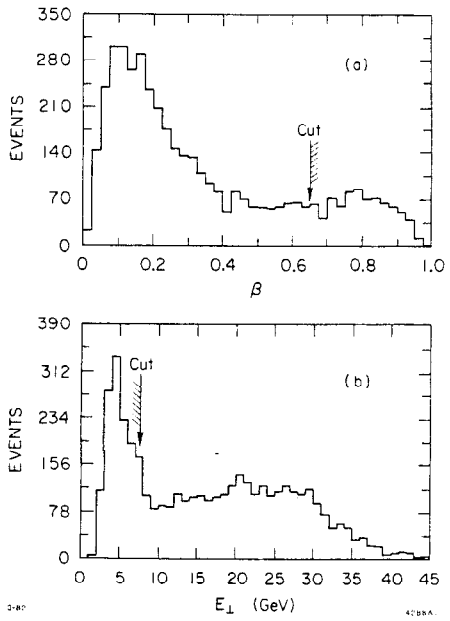

Fig. 9. (a) Imbalance and (b) $E_\perp$ distributions for all ≥5-prong events.

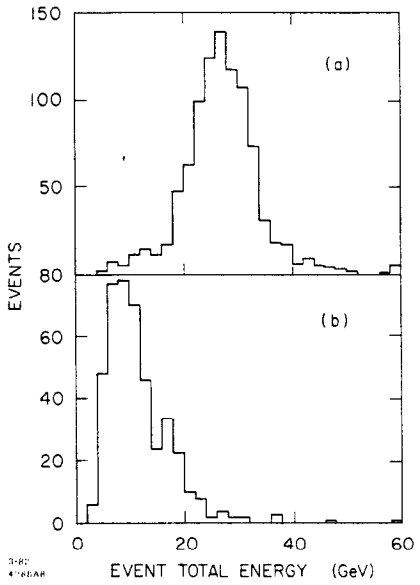

Fig. 10. (a) Events having ≥8 prongs and $\beta_z \leq 0.57$. (b) events having ≥5 prongs and $\beta_z > 0.57$.

Hadronic Energy Flow

A further objective of the study of multihadron final states is to map the distribution of energy as a function of production angle. For example, in Fig. 11 we show the distribution in polar angle of the thrust axis. The thrust T is defined by

$$T = \max \left\{ 2 \sum E_i |\cos\xi_i| / E_{cm} \right\},$$

where i runs over all energy parcels, ξ_i is the angle between the thrust axis and parcel i, and the maximization is with respect to the direction of the thrust axis. The curve in Fig. 11 represents $1 + \cos^2\theta$, the distribution expected from the quark-parton model. From Fig. 11 it is clear that the region of diminished acceptance of the calorimeter system is restricted to $|\cos\theta| > .9$, and that, barring anomolous rapid change of the true cross section very near the poles, all but six or seven percent of the integral is included in the observed distribution.

A measure of the "jettiness" of the events is the distribution in thrust, T, shown in Fig. 12 as inferred both from the calorimeter and from the charged tracks

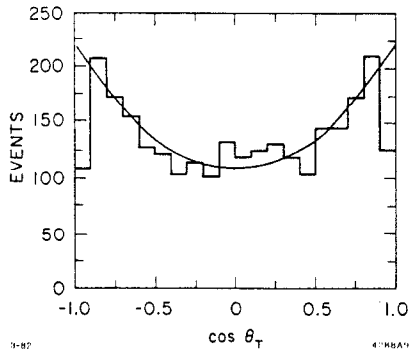

Fig. 11. Angular distribution of the thrust axis for multihadron events, determined from calorimeter energy.

seen in the central drift chamber. The calorimetric measurement appears to give a somewhat narrower peak, presumably because of the more complete sampling of the energy, but one that is displaced toward smaller average values. This may be caused by the lateral spread of the hadronic cascades which tends to produce a minimum observed jet width.

One approach to the study of energy flow in multihadron events which addresses the question of two-jet versus three-jet structure has been employed by the authors of ref. 3. A coordinate system is defined for each event such that when the angular distribution of all the energy parcels is plotted for a sample of events, the axes of two-jet events, and the production planes of three-jet events, etc., are aligned. The result is a set of three orthogonal projected energy-flow patterns as shown in Fig. 13a for our data (see ref. 3 for definitions of the major and minor axes; the thrust axis is as defined above). One can see clearly the dominant collinear two jet structure. In Fig. 13b we show the "production plane" view for events selected for maximal deviation from the two-jet character. The events appear to consist, on average, of three jets. More quantitative study is required to evaluate the significance of these features in the context of models.

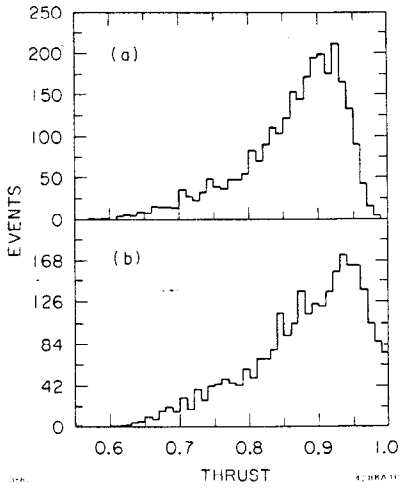

Fig. 12. Thrust distribution for multihadron events, determined from (a) calorimeter energy and (b) charged track momenta.

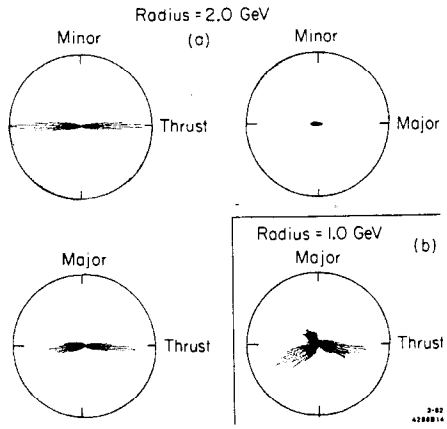

Fig. 13. (a) Energy-flow plots for the multihadron events aligned according to the directed thrust and major axes. (b) The view normal to the event plane for events having thrust ≤0.8 and oblateness ≥0.1 (see ref. 2).

Muon Identification

The calorimeter system serves also as an active filter which in combination with the muon tracking provides excellent muon identification. Preliminry data have been presented[4] on collinear QED $\mu\mu$, $\mu\mu\gamma$, and $\tau\tau \to \mu e$ events. Another example is $ee\mu\mu$ final states in which only the muons are detected; we show in Fig. 14 the invariant mass distribution for the pairs within certain fiducial cuts.

The inclusive muon distribution from multihadron events as a function of the momentum perpendicular to the thrust axis is plotted in Fig. 15. The curves show contributions from decays of known particles, and that expected from a hypothetical t-quark of mass 10 GeV having a 10% muonic branching ratio. The contribution from hadronic punch-through, which before cuts is comparable to that from π/K decay, was reduced by a factor of 5 to 10 by excluding candidates accompanied by more than 4 hits in the outer layers of the hadron calorimeter.

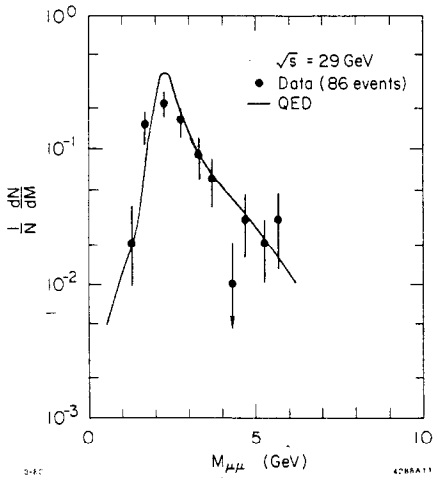

Fig. 14. Invariant mass distribution of μ pairs from $ee \to ee\mu\mu$.

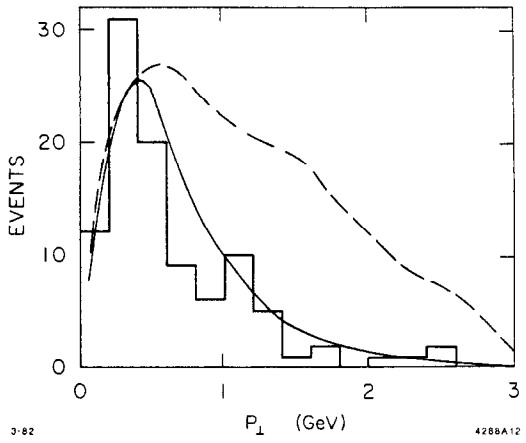

Fig. 15. Momentum perpendicular to the thrust axis for muons in multihadron events. Solid curve: calculated contribution from π, K, c, and b decay. Dashed curve: contribution of a 10-GeV t-quark with 10% muonic branching ratio.

Conclusion

The MAC detector is operating near design performance as measured in a variety of electron-positron annihilation processes at PEP. In particular, the hadron calorimeter resolution in energy and directionality agree well with calculations. The effectiveness of the large-acceptance calorimeter in detecting multihadron events has been demonstrated and precision total and differential cross section measurements can be anticipated.

References

1. R. L. Ford and W. R. Nelson, SLAC-210(1978).

2. T. A. Gabriel and B. L. Bishop, Nucl. Instr. and Methods 155,81(1978), and references therein.

3. The Mark J Collaboration, Physics Reports 63,337(1980).

4. R. Hollebeek, in Proceedings of the 1981 International Symposium on Lepton and Photon Interactions at High Energies, Bonn, Edited by W. Pfeil (Physicalisches Institut, University of Bonn,1981), p.1.